Isolated Microgrids Dominant Modes Prediction Based on Machine Learning

Mohammed Y. Morgan, Hatem F. Sindi, *Senior Member*, *IEEE*, Hatem H. Zeineldin, *Senior Member*, *IEEE*, and Ahmed Lasheen

***Abstract*—This paper employs artificial intelligence and machine learning techniques to predict the dominant oscillation modes in AC microgrids. The dominant modes are highly dependent on the droop gains and only slightly affected by the loading conditions. This paper utilizes the least absolute shrinkage and select operator (LASSO) algorithm to extract the key features contributing directly to dominant modes. The adaptive neuro-fuzzy inference system (ANFIS) is employed as a nonlinear regression technique to train a model that relates the system's key features to the dominant modes of the AC microgrid. The data obtained from a 6-bus AC microgrid test system is used to train the LASSO-based ANFIS model. The results show that the proposed method can substantially reduce the data volume of the training set due to LASSO sparse feature. The precision of the proposed algorithm is determined by comparing its output to the modes determined by the derived small-signal model of the system.**

***Index Terms*—LASSO, ANFIS, system identification islanded microgrid.**

I. Introduction

Microgrids have been introduced in recent years as an emerging technology that represents the building block in the new smart grid concept [1]. Either each microgrid can operate in islanded or grid connected mode. In islanded mode, the Distributed generation units (DGs) employ decentralized droop controllers to share active and reactive power. In this mode, voltage and frequency are governed by the system's loading conditions and droop characteristics [2]. A secondary layer oversees the primary control layer, which is responsible for restoring the voltage and frequency to their nominal values.

In addition to the steady state operation of microgrids, reliable dynamic performance also needs to be assured. Inverter-based distributed generators (IBDGs) commonly used in microgrids reduce physical inertia, and their control loop parameters can highly affect the system stability margin. Hence, it is necessary to investigate microgrids' small signal stability to ensure reliable operation during transients. Small signal analysis of a microgrid typically starts with linearizing the nonlinear model of the system around a certain operating point [3], [4]. The sensitivity analysis shows that the dominant modes are highly affected by the active droop gains and can significantly influence the system stability margin. Other studies focused on studying hybrid microgrids where the model is expanded to include both AC/DC sub-grids and interlinking converter dynamics [5], [6]. The sensitivity analysis shows that the dominant modes are highly dependent on the active droop gains of the AC subgrids.

It is essential to develop a reliable technique capable of identifying microgrid dominant modes and relating them to the system operating conditions using a suitable model. This can be highly beneficial for microgrid stability assessment in offline optimal load flow studies. In these studies, the droop gains can be used as a controlled variable to fulfill a certain objective, such as loss minimization or precise power sharing [7]. These variables should be constrained within a range that ensures microgrid stability and guarantees the operability of the optimal solution. Moreover, an online stability assessment tool can be developed by combining this model and an online estimator, such as a Kalman filter, to evaluate microgrid stability based on measured system states. If the stability margin is approached, corrective actions can be implemented to dampen the resulting oscillations and restore system stability.

Several power system identification techniques have been presented in the literature. Some techniques are

Received: July 28, 2024
Accepted: December 29, 2024
Published Online: July 1, 2025

Mohammed Y. Morgan (corresponding author) is with the Electric Power Engineering Department, Cairo University, Giza 12613, Egypt (e-mail: mohammed.yousri1 @cu.edu.eg).

Hatem F. Sindi is with the Electrical and Computer Engineering Departments, King Abdulaziz University, Jeddah 21589, Saudi Arabia (e-mail: Hfsindi@kau.edu.sa).

Hatem H. Zeineldin is with the Electric Power Engineering Department, Cairo University, Giza 12613, Egypt; and also with Khalifa University, Abu Dhabi 127788, United Arab Emirates (e-mail: hatem.zeineldin@ku.ac.ae).

Ahmed Lasheen is with the Electric Power Engineering Department, Cairo University, Giza 12613, Egypt (e-mail: Ahmed.lasheen@eng.cu.edu.eg).

DOI:10.23919/PCMP.2024.000216

based on active probing [8], which depends on perturbing the system with a well-designed input signal and measuring the corresponding output. Prony analysis [9] has been applied to earlier power systems to estimate their modal characteristics. It probes the power system using impulse excitation, and then the system equivalent model is derived from the measured responses. Steiglitz-McBride (SM) algorithm and the eigensystem realization algorithm (ERA) are reported in [10] as an alternative for the Prony method, where Prony is found to be superior to SM while ERA is recommended for its MIMO modeling capability. In [11], a subspace state space system identification algorithm is used for mode estimation. Unlike Prony analysis, it utilizes low-level probing signals.

Other data-driven modeling techniques [12] are based on artificial intelligence and deep machine learning. Linear regression is employed to predict power system oscillation modes, while in [13] it is used to predict system transient stability boundary. In [14], decision trees are used to classify the oscillation modes into well or poorly damped based on system measurements. Artificial neural network (ANN) based power oscillation identification and damping are introduced in [15], while reference [16] applies the convolutional long short-term memory 2-dimension (ConvLSTM2D) approach to estimate dominant oscillation modes based on synchrophasor data.

For microgrids, active probing or data-driven modeling techniques are applied in some researches. In [17] and [18], a real-time stability assessment approach based on subspace identification is proposed. The proposed algorithms rely on perturbing the DG active control loop, and the response is measured to identify the system-reduced order dynamic model. These approaches can only be used for online stability assessment or enhancement but cannot be applied to offline applications, as discussed previously. Data driven models based on machine learning can offer deeper insights into microgrid stability analysis, particularly due to the lower model order of microgrids compared to conventional power grids.

In [19], an ANN-based algorithm is proposed to enhance microgrid stability. The algorithm is based on creating a dataset of proportional-integral controllers, and ANN is employed to select the best one. This algorithm focuses on controller tuning, without obtaining the relationship between the system's dominant modes and the controller parameters. Reference [20] focuses on estimating the stability margin using the LASSO algorithm and ANN. However, no modeling is introduced and the scope is limited to voltage stability.

This paper employs artificial intelligence and machine learning techniques to predict the dominant modes of oscillation in AC microgrids. The main contributions of this work can be summarized as follows: 1) the use of the well-established LASSO algorithm to extract key features that directly influence the dominant modes, thereby reducing the training time; and 2) the application of ANFIS to develop a nonlinear regression model capable of predicting the system's dominant modes based on measurements of these key features.

The rest of the paper is organized as follows. Section II introduces the detailed model of an inverter-based islanded AC microgrid. An overview of LASSO and ANFIS regression techniques is presented in Section III. Section IV discusses the proposed algorithm for microgrid dominant modes identification, and the results of the proposed case studies are discussed in Section V. Finally, conclusions are stated in Section VI.

II. Isolated Microgrid Model

In this section, the dynamic model of an isolated microgrid is introduced. A typical microgrid contains it droop-based DGs, load, and lines. To obtain the complete model of the microgrid, each component needs be modeled individually, and these models are then combined to form the full model.

Figure 1 presents the different components of the AC microgrid. For ease of analysis, the system is considered a balanced three-phase system, and the *dq* frame transformation is employed to model the AC microgrid components [1].

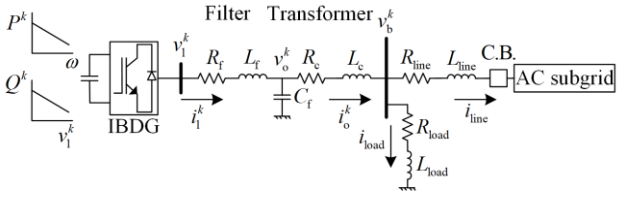

Fig. 1. AC microgrid components.

A. Inverter-based Distributed DG

In isolated AC microgrids, droop characteristics are adopted to share the active and reactive power among the system DGs, as shown in Fig. 2(a). The active and reactive power outputs of each DG are calculated using the measured output voltage and current [3]. The calculated values are then used to determine the frequency and voltage using the droop characteristics given by (1). Low-pass filters are typically employed to eliminate high-frequency harmonics in power measurements.

$$\begin{cases} \omega = m_{\mathrm{p}}(P_{\mathrm{n}}^{k} - P^{k}) \\ v_{od}^{k} = n_{q}(Q_{\mathrm{n}}^{k} - Q^{k}) \\ P^{k} = \dfrac{\omega_{\mathrm{c}}}{s+\omega_{\mathrm{c}}}(v_{od}^{k} i_{od}^{k} + v_{oq}^{k} i_{oq}^{k}) \\ Q^{k} = \dfrac{\omega_{\mathrm{c}}}{s+\omega_{\mathrm{c}}}(v_{od}^{k} i_{od}^{k} - v_{oq}^{k} i_{oq}^{k}) \end{cases} \tag{1}$$

where ω is the AC side frequency; while $m_{\mathrm{p},k}^{\mathrm{ac}}$ and $n_{q,k}$ are IBDG droop gains; P_{n}^{k} and Q_{n}^{k} are the no-load reference for active and reactive loops; P^{k} and Q^{k} are the output active and reactive power from IBDG of bus k; ω_{c} is the cut-off frequency of the filters; i_{odq}^{k} and v_{odq}^{k} are the dq components of the output voltage and current of the LC filter connected to the kth IBDG.

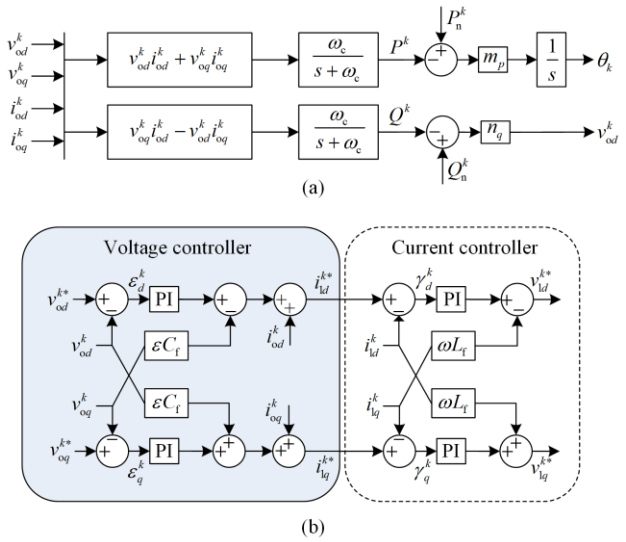

Fig. 2. IBDG controllers. (a) Power controller. (b) Voltage and current controllers.

The voltage and current controllers shown in Fig. 2(b) can be modeled as:

$$\begin{cases} \dot{\epsilon}_d^k = v_{od}^{k*} - v_{od}^k \\ \dot{\epsilon}_q^k = v_{oq}^{k*} - v_{oq}^k \\ \dot{\gamma}_d^k = i_{ld}^{k*} - i_{ld}^k \\ \dot{\gamma}_q^k = i_{lq}^{k*} - i_{lq}^k \\ i_{ld}^* = (K_{\mathrm{iv}}\epsilon_d^k + K_{\mathrm{pv}}\dot{\epsilon}_d^k - \omega C_{\mathrm{f}} v_{oq}^k + i_{od}^k) \\ i_{lq}^* = (K_{\mathrm{iv}}\epsilon_q^k + K_{\mathrm{pv}}\dot{\epsilon}_q^k - \omega C_{\mathrm{f}} v_{oq}^k + i_{oq}^k) \\ v_{ld}^k = K_{\mathrm{ic}}\gamma_d^k + K_{\mathrm{pc}}\dot{\gamma}_d^k - \omega L_{\mathrm{f}} i_{oq}^k \\ v_{lq}^k = K_{\mathrm{ic}}\gamma_q^k + K_{\mathrm{pc}}\dot{\gamma}_q^k - \omega L_{\mathrm{f}} i_{od}^k \end{cases} \tag{2}$$

where v_{ldq}^k and i_{ldq}^k are dq components of the terminal voltage and current of the kth IBDG while v_{lq}^{k*} and i_{ld}^{k*} are their reference values; ϵ_{dq}^k and γ_{dq}^k are intermediate variables of the voltage and current controllers; K_{pv} and K_{iv} are the proportional and integral gains of the inner control loops; L_{f}, R_{f} and C_{f} the parameters of the LC filter.

The coupling filter and transformer between the IBDG and the AC subsystem can be modeled by:

$$\begin{cases} \dot{i}_{ld}^k = \omega_{\mathrm{base}}\left(\dfrac{-R_{\mathrm{f}}}{L_{\mathrm{f}}} + \omega i_{lq}^k + \dfrac{1}{L_{\mathrm{f}}}(v_{ld}^{k*} - v_{od}^k)\right) \\ \dot{i}_{lq}^k = \omega_{\mathrm{base}}\left(\dfrac{-R_{\mathrm{f}}}{L_{\mathrm{f}}} i_{lq}^k - \omega i_{ld}^k + \dfrac{1}{L_{\mathrm{f}}}(v_{lq}^{k*} - v_{oq}^k)\right) \\ \dot{v}_{od}^k = \omega_{\mathrm{base}}\left(\omega i_{oq}^k + \dfrac{1}{L_{\mathrm{f}}}(i_{ld}^k - i_{od}^k)\right) \\ \dot{v}_{oq}^k = \omega_{\mathrm{base}}\left(-\omega i_{od}^k + \dfrac{1}{C_{\mathrm{f}}}(i_{lq}^k - i_{oq}^k)\right) \\ \dot{i}_{ld}^k = \omega_{\mathrm{base}}\left(\dfrac{-R_{\mathrm{c}}}{L_{\mathrm{c}}} i_{od}^k + \omega i_{oq}^k + \dfrac{1}{L_{\mathrm{c}}}(v_{od}^k - v_{bd}^k)\right) \\ \dot{i}_{oq}^k = \omega_{\mathrm{base}}\left(\dfrac{-R_{\mathrm{c}}}{L_{\mathrm{c}}} i_{oq}^k - \omega i_{od}^k + \dfrac{1}{L_{\mathrm{c}}}(v_{oq}^k - v_{bq}^k)\right) \end{cases} \tag{3}$$

where R_{c} and L_{c} represent the series impedance of the coupling transformer; $v_{\mathrm{b}dq}^k$ are dq components of the kth bus in the AC subgrid; and ω_{base} is the base frequency.

B. Network and Load Model

Short lines and constant impedance models are adopted to represent the AC lines and loads, respectively, with both lines and loads modeled as a series R-L circuits. The mathematical models described in the dq frame are given by:

$$\begin{cases} v_d^{\mathrm{line}} = R^{\mathrm{line}} i_d^{\mathrm{line}} + L^{\mathrm{line}} \dfrac{\mathrm{d}}{\mathrm{d}t} i_d^{\mathrm{line}} - \omega L^{\mathrm{line}} i_q^{\mathrm{line}} \\ v_q^{\mathrm{line}} = R^{\mathrm{line}} i_q^{\mathrm{line}} + L^{\mathrm{line}} \dfrac{\mathrm{d}}{\mathrm{d}t} i_q^{\mathrm{line}} - \omega L^{\mathrm{line}} i_d^{\mathrm{line}} \end{cases} \tag{4}$$

$$\begin{cases} v_d^{\mathrm{load}} = R^{\mathrm{load}} i_d^{\mathrm{load}} + L^{\mathrm{load}} \dfrac{\mathrm{d}}{\mathrm{d}t} i_d^{\mathrm{load}} - \omega L^{\mathrm{load}} i_q^{\mathrm{load}} \\ v_q^{\mathrm{load}} = R^{\mathrm{line}} i^{\mathrm{load}} + L^{\mathrm{load}} \dfrac{\mathrm{d}}{\mathrm{d}t} i_q^{\mathrm{load}} - \omega L^{\mathrm{load}} i_d^{\mathrm{load}} \end{cases} \tag{5}$$

C. Overall Model

The dq frame is adopted to model the microgrid. Each component is modeled to its reference frame. It is a common practice to choose one DG's dq frames as a reference frame and to convert all the variables from each model to this common frame [4]. The angle difference between this frame and other frames is given by:

$$\delta = \int (\omega - \omega_{\mathrm{com}})\mathrm{d}t \tag{6}$$

where ω_{com} is the speed of the common reference dq frame.

The complete system model can be obtained by combining the individual models of the aforementioned subsystems. Figure 3 represents the block diagram of the complete system model and illustrates the interconnection between the different subsystems.

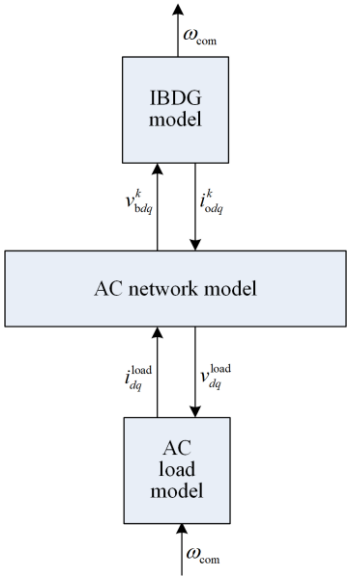

Fig. 3. Overall system model.

III. Machine Learning Overview

This section presents an overview of machine learning methods that will be used to identify the microgrid dominant modes of oscillations as a function of the microgrid drop gains and operating conditions.

The system identification problem can be transformed into a machine-learning problem in which the training data set can be of the form:

$$D_n = \{(\boldsymbol{X}_1, Y_1), (\boldsymbol{X}_2, Y_2), \cdots, (\boldsymbol{X}_n, Y_n)\} \tag{7}$$

where $\boldsymbol{X}$ represents the system inputs (features) vector while Y represents the corresponding output (response). It is required to obtain a certain model that represents the relationship between the given features and the required observation or output. The model is trained using the available training data set to minimize the error between the given observations and the values predicted by the model. The model can be linear or of higher order according to the relationship nature.

A. LASSO Regression

The "least absolute shrinkage and selection operator" was first introduced in the late 1990s [21]. The algorithm was developed to solve the overfitting problem related to the linear regression problem of the form:

$$Y = \sum_{j=1}^{p} \beta_j X^{(j)} + \varepsilon \tag{8}$$

where β_j is the weighting factor; and ε represents the system noise. To overcome the overfitting problem, not only minimizes the least square error but also introduces an additional penalty term given by:

$$\hat{\boldsymbol{\beta}}_{\text{LASSO}} = \arg\min_{\boldsymbol{\beta}} \left(\frac{1}{n} \|\boldsymbol{Y} - \boldsymbol{X}\boldsymbol{\beta}\|_2^2 + \lambda \sum_{j=1}^{p} |\beta_j| \right) \tag{9}$$

where λ is a regularization parameter that needs to be specified. It controls the amount of shrinkage in the minimization criterion. In practice, one can select λ according to some resampling methods, i.e., crossvalidation. It must be noted that an earlier version of the enhanced minimization criterion is introduced by the ridge formula [22], given by:

$$\hat{\boldsymbol{\beta}}_{\text{ridge}} = \arg\min_{\boldsymbol{\beta}} \left(\frac{1}{n} \|\boldsymbol{Y} - \boldsymbol{X}\boldsymbol{\beta}\|_2^2 + \lambda \sum_{j=1}^{p} |\beta_j^2| \right) \tag{10}$$

As shown in (9) and (10), the main difference between the two approaches is characterized by the penalty term. LASSO's approach employs the L1 norm of the weights rather than the L2 norm utilized by the ridge regression.

Using the L1 norm can be beneficial as it allows some of the features to have zero weights in the regression model. In contrast, ridge regression, which employs the L2 norm, does not produce sparse solution. This sparse property associated with the LASSO algorithm can improve model accuracy and help eliminate irrelevant features, particularly in high-dimension problems. This extends the applications of LASSO in machine learning not only for linear regression but also for feature selection. Employing the LASSO selection property can significantly reduce the number of system features with minimum impact on prediction accuracy, resulting in lower computation complexity and higher efficiency [20]. In this paper, LASSO is introduced as a feature selection method to enhance the efficiency of the microgrid dominant modes estimation algorithm, as will be discussed later.

The closed-form formula for both least square and ridge regression can be given by:

$$\hat{\boldsymbol{\beta}}_{\text{Least}} = (\boldsymbol{X}^{\text{T}}\boldsymbol{X})^{-1}(\boldsymbol{X}^{\text{T}}\boldsymbol{Y}) \tag{11}$$

$$\hat{\boldsymbol{\beta}}_{\text{ridge}} = (\boldsymbol{X}^{\text{T}}\boldsymbol{X} + n\lambda\boldsymbol{I}_p)^{-1}(\boldsymbol{X}^{\text{T}}\boldsymbol{Y}) \tag{12}$$

where $\boldsymbol{I}_p$ is $p \times p$ identity matrix.

Unfortunately, there is no closed-form solution for LASSO regression. Instead, the weights are typically computed using coordinate algorithms, often referred to as "shooting algorithms", which iteratively solve the underlying optimization problem [23]. The advantages of LASSO over other machine learning methods can be summarized as follows:

1) Interpretability. Since LASSO reduces the number of non-zero features; the final model is simpler and more interpretable. For example, decision trees or random forests can also provide a ranking of features by importance. LASSO provides more interpretable linear relationships and often leads to faster feature selection on larger datasets.

2) Selection efficiency. Unlike some other variable selection algorithms such as recursive feature elimi-

nation (RFE) or stepwise regression, LASSO is computationally efficient and provides much-I proved scaling to datasets with a high number of features.

3) Prevents overfitting. LASSO penalizes the size of the coefficients, hence reducing the chances of overfitting in models with large numbers of features. This help retain only the most predictive features, thereby enhancing the model's ability to generalize to unseen data.

B. ANFIS Regression

Fuzzy systems can turn knowledge gained by experience into rule-based models useful in system identification and control. Fuzzy modeling is beneficial for dealing with complex and multidimensional systems. A fuzzy inference system (FIS) model can be built to establish adequate rules and membership functions to correctly model the system. Fuzzy systems offer several advantages over neural networks when it comes to modeling, including the following:

1) The ability to infer the relationship between imprecise and ambiguous input data and effect (output) [24].

2) Can easily overcome the overfitting problem and provide better prediction capability [25].

To combine the learning capabilities of ANN and the advantage of the fuzzy systems, ANFIS is introduced in [26]. The inference system consists of a set of fuzzy based rules, which can be given by:

$$\begin{cases} \mathrm{R}_1: \text{if } x \text{ is } \mathrm{A}_1 \text{ and } y \text{ is } \mathrm{B}_1 \text{ then } z_1 = p_1 x + q_1 y + r_1 \\ \mathrm{R}_2: \text{if } x \text{ is } \mathrm{A}_1 \text{ and } y \text{ is } \mathrm{B}_2 \text{ then } z_2 = p_2 x + q_2 y + r_2 \\ \mathrm{R}_3: \text{if } x \text{ is } \mathrm{A}_2 \text{ and } y \text{ is } \mathrm{B}_1 \text{ then } z_3 = p_3 x + q_3 y + r_3 \\ \mathrm{R}_4: \text{if } x \text{ is } \mathrm{A}_2 \text{ and } y \text{ is } \mathrm{B}_2 \text{ then } z_4 = p_4 x + q_4 y + r_4 \end{cases} \tag{13}$$

The structure of the ANFIS network, as shown in Fig. 4, is based on five main layers [27]:

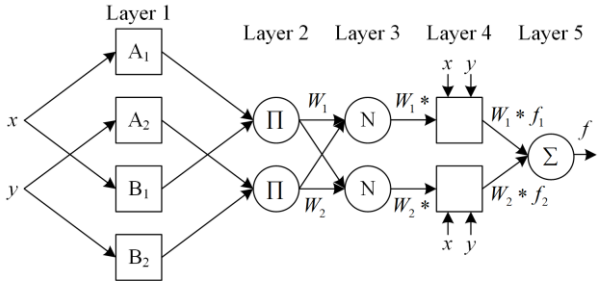

Fig. 4. Overall system model.

Layer 1: It represents the input layer and consists of adaptive nodes. The fuzzification of the inputs takes place in this layer through (14).

Layer 2: This layer (rule nodes layer) contains the fuzzy rules, and its output represents the rule's firing strength given by (15).

Layer 3: This layer calculates the normalized firing strengths of previous rule nodes using (16).

Layer 4: This node is responsible for calculating the contribution of each rule into the final output using (17).

Layer 5: This is the output layer where the defuzzification of the inputs occurs, and (18) give the final output.

$$\begin{aligned} O_i^1 &= \mu_{A_i}(x), \ i = 1, 2 \\ O_i^1 &= \mu_{B_{i-2}}(x), \ i = 3, 4 \end{aligned} \tag{14}$$

$$O_k^2 = w_k = \mu_{A_i}(x)\mu_{B_j}(x), \ i, j, k = 1, 2 \tag{15}$$

$$O_i^3 = \overline{w}_i = \frac{w_i}{\sum_{i=1}^{4} w_k}, \ i = 1, 2 \tag{16}$$

$$O_i^4 = \overline{w}_i x_i = \overline{w}_i (p_i x + q_i y + r_i), \ i = 1, 2 \tag{17}$$

$$O_i^5 = \sum_{i=1}^{2} \overline{w}_i f_i \tag{18}$$

The advantages make the ANFIS a universal estimator capable of predicting specific features under varying operating conditions. This property is particularly valuable in this research, as it enhance the accuracy of oscillatory modes prediction across different droop gains and loading conditions [27], [28].

IV. Selection and Training Algorithm

This section presents the proposed steps including data set generation, the LASSO selection algorithm, and finally the ANFIS training procedures.

A. Generation of the Training Data

To generate the data for training the prediction model, the following steps are undertaken. First, the active droop gains are assumed to be the same for all DGs to ensure equal load sharing and system stability (base case). The droop gains are then increased equally from the base case value to a value that causes the system to operate around the stability limits. This make the system modes move from their base case values to those close to instability. Active droop gains used during the training process can be written as:

$$m_{\mathrm{p}} = m_{\mathrm{p}}^0 (1 + \Delta m_{\mathrm{p}}) \tag{19}$$

where m_{p}^0 and Δm_{p} are the base case active droop gains and the percentage of perturbation of active droop gain allowed in each DG.

To broaden the range of the prediction model, the loading of the microgrid is taken into consideration. While loading only has small effect on the mode locations [3], the model prediction accuracy can be enhanced by incorporating the microgrid loading condition. For this purpose, the microgrid loading is randomly changed within ±50% variations from the base case at each value of the active droop gain. Since this

work assumed a constant impedance model to represent the load, the load adjustment scheme can be given by:

$$\begin{aligned} R_i^{\text{load}} &= R_{\text{o}}^{\text{load}}(1+\Delta R_i^{\text{load}}) \\ L_i^{\text{load}} &= L_{\text{o}}^{\text{load}}(1+\Delta L_i^{\text{load}}) \end{aligned} \tag{20}$$

where $R_{\text{o}}^{\text{load}}$ and $L_{\text{o}}^{\text{load}}$ represent the nominal impedance of the ith load in the base case; while ΔR_i^{load} and ΔL_i^{load} are the allowable percentage perturbation in the ith load impedance.

The next step is to linearize the system around each operating point to obtain the system state matrix and the corresponding Eigenvalues of the dominant mode. The linearization process is done using the Matlab "linear analysis toolbox." The output system model is given in the form:

$$\begin{cases} \Delta\dot{x}(t) = A\Delta x(t) + B\Delta u(t) \\ \Delta y(t) = C\Delta x(t) + D\Delta u(t) \end{cases} \tag{21}$$

The system states represent the inputs to the prediction model, while the dominant mode Eigenvalues are the corresponding outputs. The operating points are a different combination of active droop gains and loading conditions. Hence, each operating point represents the system status at specific loading and droop gain.

B. LASSO Selection Algorithm

The number of the generated data sets is equal to the number of the loading conditions multiplied by the number of the active droop gain values. Each data set represents a pair of the system states and the mode location. The LASSO shooting algorithm is employed to determine the weight that corresponds to each of these states. LASSO can determine the states which have the minimal effect on the prediction of the dominant mode and then force them to zero. This minimizes the number of states and, hence, the size of the training data. Moreover, the structure of the corresponding ANFIS network is substantially reduced, which speeds up the training process. The LASSO feature selection algorithm can be summarized in the following steps: 1) normalize the data set; 2) divide the Data set into k folds; 3) calculate the regularization parameter using cross validation; 4) determine the weights of the input states; and 5) select the inputs of non-zero weights.

C. ANFIS Training

After selecting the effective states using the LASSO algorithm, the revised data set is used for training the ANFIS model. The data are divided into training, checking, and validation data sets. The training data set is used in ANFIS training, while the ANFIS learning algorithm combines a backpropagation gradient with a forward pass for each training iteration (epoch). The descent algorithm employs the least-squares estimator. After presenting an input vector, node outputs proceed until layer four, where the resulting parameters can be identified using the least-squares approach. The gradient descent technique updates the network parameters as the error signals propagate backward in the backward step.

In this stage, the resulting parameters are fixed. The checking data set is used to help prevent ANFIS training from overfitting. The validation data set is used to validate the model and evaluate the model prediction accuracy. For the final step, the validation data set is used to validate the model and evaluate the model's prediction accuracy. The validation data set allows testing of each FIS model at this level. Two well-known performance measures, the root mean square error (RMSE) and mean absolute square error (MASE), are devised as criteria for selecting the best FIS models. The initial Sugeno-type FIS models are constructed using the training data set and the subtractive clustering approach [27]. Among clustering algorithms, this approach has the advantage that its simplicity is proportional to the quantity of data points and is independent of the problem's dimension.

The eigenvalues of the dominant modes consist of real and imaginary parts, which have different relations to the system states. Hence, two distinct ANFIS models are used to predict the real and imaginary parts. Similarly, the LASSO selection algorithm is used to select the dominant features for each model.

It must be noted that the proposed algorithm has many advantages over sensitivity analysis in identifying the system's dominant modes. Sensitivity analysis requires varying each parameter to estimate its impact, possibly without directly eliminating irrelevant features and thus can be computationally expensive in case of a high number of parameters. In contrast, the proposed algorithm utilizes a computationally efficient LASSO technique to enhance feature selection. Sensitivity analysis, by its very nature, does not consider parameter correlation while looks at each input variable in isolation. Therefore, when multiple inputs are interrelated, it becomes challenging to determine which parameter is truly dominant or how their interactions influence the system. Moreover, non-linearity can cause problems unless more advanced global sensitivity methods are applied, which again increase computational costs. On the other hand, the proposed algorithm utilized ANFIS, which can handle various types of nonlinearity due to ANN, while its fuzzy inference system captures complex relationships between system inputs and outputs.

V. Case Studies

This system presents the case studies used for testing and validation of the proposed prediction model.

A. Test System

The system under study is an AC microgrid with a 6-bus, as shown in Fig. 5. The microgrid operates in islanded mode with three droop-based DGs and two

loads. The parameters of the test system can be found in [4]. As stated previously, the three DGs have the same active droop gains to ensure equal power sharing. The active droop gain of the base case is chosen to be 0.003 p.u while their loads are represented by equivalent resistances of 20 Ω and 25 Ω, respectively. The system modes are obtained by calculating the eigenvalues of the state matrix A of the linearized system around the base case operating point. It was found that the system has 45 states and eigenvalues. The critical modes of oscillation of the linearized system can be found in Table I.

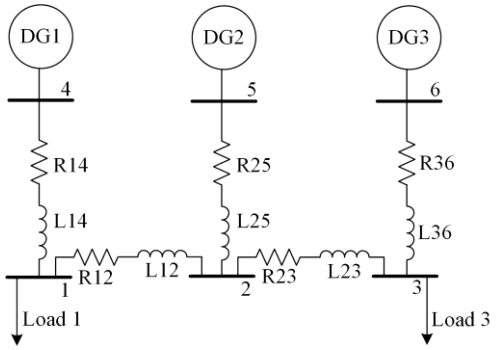

Fig. 5. The 6-bus test system.

TABLE I
DOMINANT MODES OF THE TEST SYSTEM

	Real (/s)	Imag. (rad/s)	Damping ratio (%)	Natural frequency (Hz)
Mode 1	−8.836	±48.21	18	49
Mode 2	−13.8	±22.65	52	26.5

B. LASSO Selection Algorithm Verification

The linearized model contains a large number of states that are used as input to the prediction model. Hence, the LASSO selection algorithm is applied to eliminate the states that have low contributions to the system's dominant eigenvalues.

Ninety-seven operating points are generated, which corresponds to changing the active droop gains from 0.003 to 0.006. Figure 6 depicts the movement of the dominant modes towards instability when changing the active droop gains.

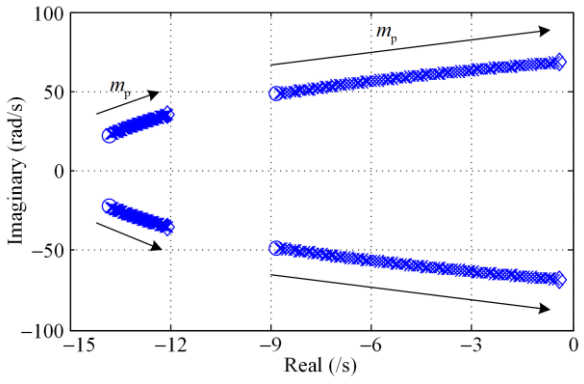

Fig. 6. The trajectory of the dominant modes while changing mp.

It can be seen from Table I that mode 1 is more dominant than mode 2. Hence, the proposed prediction model considers mode 1 as the required output. After optimizing the regularization parameter λ to remove the redundant features, the final selected features only have 4 and 5 states for predicting the real and imaginary parts of the eigenvalue, respectively. The weights of these states are demonstrated in Fig. 7 and are listed in Table II.

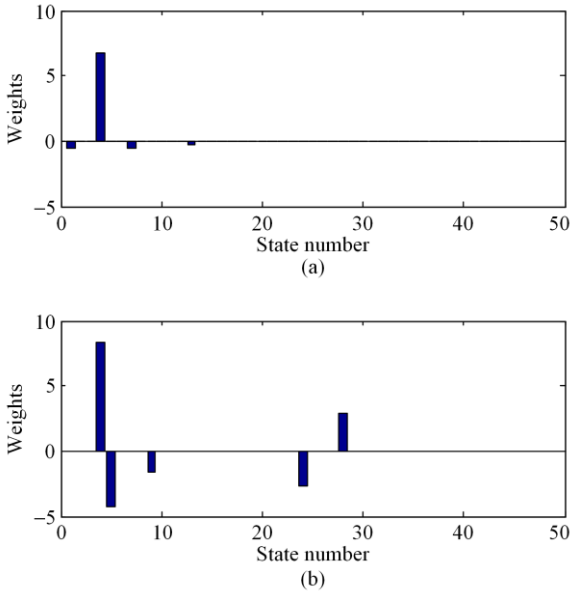

Fig. 7. Weights of the dominant states in Eigenvalues. (a) Real part. (b) Imaginary part.

TABLE II
SELECTED STATES BASED ON THE LASSO ALGORITHM

Real part selected states		Imaginary part selected states	
State	Weight	State	Weight
δ^1	−0.617	ϵ_d^1	8.30
ϵ_d^1	6.70	ϵ_q^1	−4.23
Q^1	−0.567	Q^1	−1.67
λ_d^1	−0.346	i_{oq}^2	−2.62
		v_{od}^2	2.88

Figure 8 depicts the correlations between the real part of the 48 Hz mode and the top four dominant states, which greatly match the weight of the states selected by LASSO and listed in Table II. The same consistency can be found for the selected states for the predicted imaginary part. For further validation, the selected features are used to estimate the mode location for the same change in the active droop gains. A comparison between the actual and estimated values is demonstrated in Fig. 9. The calculated MAPE is 3.5% and 0.61%, while RMSE is 0.0757 and 0.424 for real and imaginary parts, respectively.

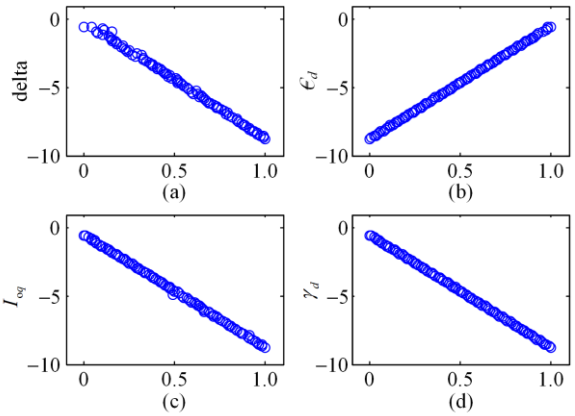

Fig. 8. The real part of the dominant mode versus the top selected states.

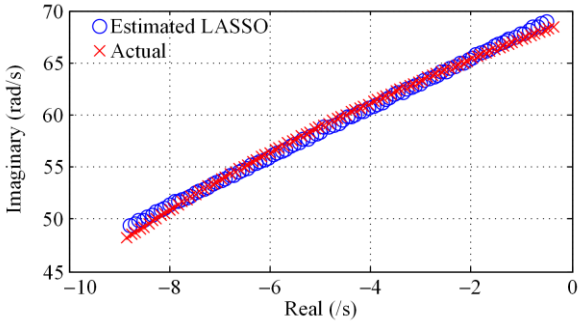

Fig. 9. LASSO regression of the dominant modes.

C. ANFIS Model Testing: Single Loading Condition

Two ANFIS models are employed to predict the real and imaginary parts of the eigenvalue, which corresponds to the dominant mode (using Matlab fuzzy toolbox).

Each ANFIS model acquires its optimal inputs from the preceding LASSO selection algorithm. Subtractive clustering is used to determine the initial FIS with six membership functions for each input. The same generated data set used for feature selection is used to tune the ANFIS models with 70%, 15%, and 15% of the data used for training, checking, and testing, respectively. The number of epochs required for training the two ANFIS models is approximately 100 for both models.

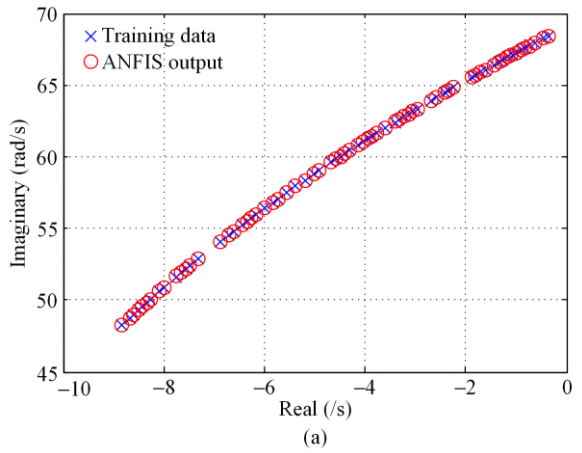

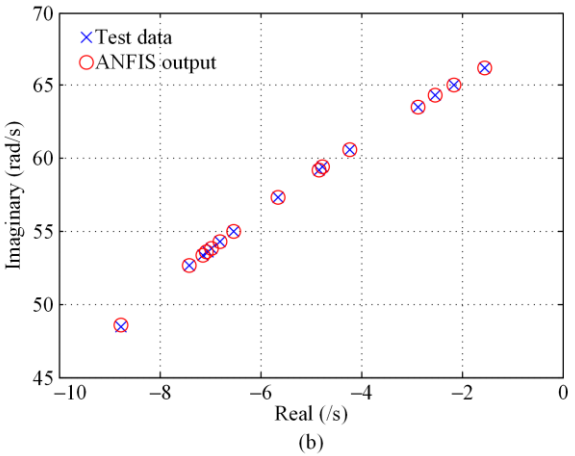

Fig. 10. Dominant mode actual and estimated locations. (a) Training data. (b) Test data.

The RMSE of the trained models are 0.0008 and 0.0029. Figure 10 depicts the actual versus estimated locations of the dominant mode. The results demonstrate the capability of ANFIS to model the nonlinear relation between the inputs and outputs with minimum error compared to LASSO linear regression in Fig. 9. The output Sugeno-type fuzzy rules are presented in Fig. 11.

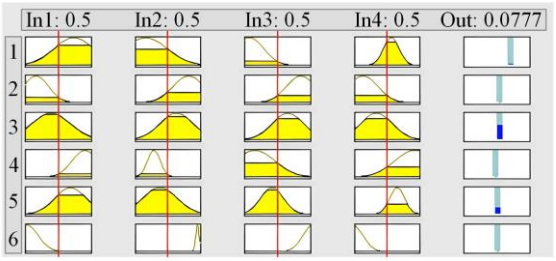

Fig. 11. ANFIS model fuzzy rules.

D. Multiple Loading Conditions

In this test case, the system loading condition is taken into consideration while generating the training data set. While adjusting the active droop gain in the previous range, the microgrid loading is changed at each gain value within ±50% variations from the base case. The load variation range is divided into steps resulting in 12 loading conditions in total. Figure 12 depicts the actual versus estimated values of the Eigenvalues of the dominant mode when 12 loading conditions are used to train the models.

Table III presents the data size and the statistics of the models trained at the specified loading conditions. It can be shown that the error increases as the number of samples increases, which represents more loading cases. Compared to the single loading case, three new inputs are added to the real part model, while only two inputs are added to the imaginary part model. The new inputs appeared due to the microgrid loading effect, while the number of inputs is much lower than the total system states, due to the LASSO feature selection.

Moreover, the number of fuzzy rules is reduced as the number of loading conditions increases. The correlation between the microgrid loading and the dominant mode location becomes stronger when more loading conditions are introduced. Hence, fewer fuzzy rules are required.

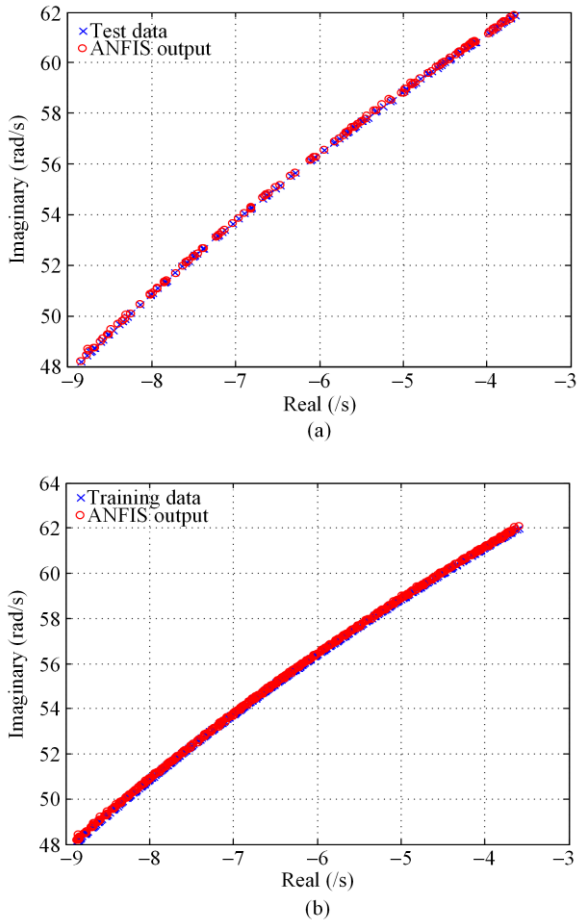

Fig. 12. Dominant mode actual and estimated locations for multiple loading conditions. (a) Training data. (b) Test data.

TABLE III
ANFIS RESULTS FOR MULTIPLE LOADING CONDITIONS

Loading conditions	Data size	Model 1			Model 2		
		Inputs	Rules	RMSE	Inputs	Rules	RMSE
3	180	7	11	0.000 338	7	12	0.0016
6	360	7	10	0.0005	7	9	0.0037
9	540	7	9	0.001 78	7	9	0.0057
12	720	7	7	0.0037	8	7	0.022

VI. CONCLUSION

In this paper, a machine learning-based method is proposed to predict the location of the dominant modes in isolated droop-based microgrids. The proposed method employs the LASSO selection algorithm to eliminate the redundant features and minimize the number of inputs to the ANFIS model. To ensure accurate estimation of the mode location regardless of the nonlinearity of the system, two ANFIS models are presented to predict the real and imaginary parts of the corresponding Eigenvalues. The models are trained at different operating points, including different droop gains, and loading conditions. The agreement of the proposed method results with the results from the small signal analysis demonstrates the accuracy and robustness of the proposed method. Hence, it represents a powerful tool for planning the operation of droop based microgrids.

ACKNOWLEDGMENT

Not applicable.

AUTHORS' CONTRIBUTIONS

Mohamed Y. Morgan: writing-original draft, supervision, methodology, and conceptualization. Hatem F. Sindi: writing-review & editing, validation, supervision, and conceptualization. Hatem H. Zeineldin: writing-review & editing, supervision, methodology, and conceptualization. Ahmed Lasheen: writing-review & editing, validation, methodology, and conceptualization. All authors read and approved the final manuscript.

FUNDING

This work is supported by the Deanship of Scientific Research (DSR) at King Abdulaziz University (KAU), Jeddah, Saudi Arabia (No. GPIP: 676-135-2024).

AVAILABILITY OF DATA AND MATERIALS

Please contact the corresponding author for data material request.

DECLARATIONS

Competing interests: The authors declare that they have no known competing financial interests or personal relationships that could have appeared to influence the work reported in this article.

AUTHORS' INFORMATION

Mohammed Y. Morgan received the B.Sc. and M.Sc. degrees in electrical engineering from Cairo University, Giza, Egypt, in 2009 and 2013, respectively, and the Ph.D. degree in electric power engineering from the Cairo University, Giza, Egypt, in 2018. He is an assistant professor in the Department of Electric Power Engineering Department at Cairo University, Giza, Egypt. His research interests include smart grids, distributed generation, micro grids and power system stability.

Hatem F. Sindi received the B.Sc. degree in electrical engineering from King Abdulaziz University, Jeddah, Saudi Arabia, in 2007, and the M.Sc. and Ph.D. degrees in electrical engineering from the University of Waterloo, Waterloo, ON, Canada, in 2013 and 2018, respectively. He is an assistant professor in the Department of Electrical and Computer Engineering at King Abdulaziz University, Jeddah, Saudi Arabia. His research interests include smart grid, renewable DG, distribution system planning, electric vehicles, storage systems, and bulk power system reliability.

Hatem H. Zeineldin received the B.Sc. and M.Sc. degrees in electrical engineering from Cairo University, Giza, Egypt, in 1999 and 2002, respectively, and the Ph.D. degree in electrical and computer engineering from the University of Waterloo, Waterloo, ON, Canada, in 2006. He was with Smith and Andersen Electrical Engineering, Inc., North York, ON, USA, where he was involved in projects involving distribution system designs, protection, and distributed generation. He was a Visiting Professor with the Massachusetts Institute of Technology, Cambridge, MA, USA. He is with Khalifa University of Science and Technology, Abu Dhabi, UAE and on leave from Faculty of Engineering, Cairo University. His current research interests include distribution system protection, distributed generation, and micro grids. He is currently an Editor for the IEEE Transactions on Energy Conversion.

Ahmed Lasheen was born in Giza, Egypt Graduated from Cairo University, in 2010. He received the M.Sc. and Ph.D degrees in electrical engineering from Cairo University, Giza, Egypt, in 2013 and 2017, respectively. Currently, he is an associate professor with Cairo University. His current research interests include wind energy conversion system, microgrids, model predictive control, fuzzy control, adaptive control, autonomous vehicles, and neural networks.

REFERENCES

[1] N. Hatziargyriou, "Microgrids: architectures and control" Wiley-IEEE, UK., 2014.

[2] D. E. Olivares, A. Mehrizi-Sani, and A, H. Etemadi *et al*., "Trends in microgrid control," *IEEE Transactions on Smart Grid*, vol. 5, no. 4, pp. 1905-1919, Jul. 2014.

[3] N. Pogaku, M. Prodanović, and T. C. Green, "Modeling, analysis and testing of autonomous operation of an inverter-based microgrid," *IEEE Transactions on Power Electronics*, vol. 22, no. 2, pp. 613-625, Mar. 2007.

[4] M. Rasheduzzaman, J. A. Mueller, and J. W. Kimball, "Reduced-order small-signal model of microgrid systems," *IEEE Transactions on Sustainable Energy*, vol. 6, no. 4, pp. 1292-1305, Mar. 2015.

[5] D. Espín-Sarzosa, R. Palma-Behnke, and C. A. Cañizares *et al*., "Microgrid modeling for stability analysis," *IEEE Transactions on Smart Grid*, vol. 15, no. 3, pp. 2459-2479, May 2024.

[6] A. A. Eajal, A. Aderibole, and H. Muda *et al*., "Stability evaluation of AC/DC hybrid microgrids considering bidirectional power flow through the interlinking converters," IEEE Access, vol. 9, p. 43876-43888, Mar. 2021.

[7] A. A. Eajal, A. H. Yazdavar, and E. F. El-Saadany *et al*., "Optimizing the droop characteristics of AC/DC hybrid microgrids for precise power sharing," *IEEE Systems Journal*, vol. 15, no. 1, pp. 560-569, Mar. 2021.

[8] R. Chakraborty, H. Jain, and G. S. Seo, "A review of active probing-based system identification techniques with applications in power systems," *International Journal of Electrical Power & Energy Systems*, vol. 140, Sept. 2022.

[9] K. Rao and K. N. Shubhanga, "A comparison of SVD-augmented prony algorithms for noisy power system signals," in *IEEE Access*, vol. 11, pp. 143457-143474, Dec. 2023.

[10] J. J. Sanchez-Gasca and J. H. Chow, "Performance comparison of three identification methods for the analysis of electromechanical oscillations," *IEEE Transactions on Power Systems*, vol. 14, no. 3, pp. 995-1002, Aug. 1999.

[11] F. Al Hasnain, M. S. Hasan, and M. H. Arifin *et al*., "Oscillation identification and frequency damping controller design for battery energy storage system using subspace identification," *IEEE Transactions on Industry Applications*, vol. 60, no. 3, pp. 4796-4809, May 2024.

[12] W. Mo, J. Lü, and M. Pawlak *et al*., "Power system oscillation mode prediction based on the Lasso method," *IEEE Access*, vol. 8, pp. 101068-101078, 2020.

[13] A. Ingalalli and S. Kamalasadan, "Data-driven decentralized online system identification-based integral model-predictive voltage and frequency control in microgrids," *IEEE Transactions on Industrial Informatics*, vol. 20, no. 2, pp. 1963-1974, Feb. 2024

[14] P. McNabb, D. Wilson, and J. Bialek, "Classification of mode damping and amplitude in power systems using synchrophasor measurements and classification trees," *IEEE Transactions on Power Systems*, vol. 28, no. 2, pp. 1988-1996, May 2013.

[15] Z. Huang, N. Zhou, and F. K. Tuffner *et al*., "Mango modal analysis for grid operation: a method for damping improvement through operating point adjustment," Pacific Northwest National Lab (PNNL), Richland, WA (United States), 2010.

[16] F. Senesoulin, I. Ngamroo, and S. Dechanupaprittha, "Estimation of dominant power oscillation modes based on CONVLSTM approach using synchrophasor data and cross-validation technique," *Sustainable Energy, Grids and Networks*, vol. 31, Sept. 2022.

[17] A. El-Hamalawy, M. Ammar, and H. Sindi *et al*., "A subspace identification technique for real-time stability assessment of droop based microgrids," *IEEE Transac-*

tions on Power Systems, vol. 37, no. 4, pp. 2731-2743, Jul. 2022.

[18] P. N. Papadopoulos, T. A. Papadopoulos, and P. Crolla *et al*., "Measurement-based analysis of the dynamic performance of microgrids using system identification techniques," *IET Generation*, *Transmission and Distribution*, vol. 9, no. 1, pp. 90-103, Jan. 2015.

[19] A. K. Venkatesan U. Subramaniam, and M. S. Bhaskar *et al*., "Small-signal stability analysis for microgrids under uncertainty using MALANN control technique," *IEEE System Journal*, vol. 15, no. 3, pp. 3797-3807, Sept. 2021.

[20] Y. Tang, K. Tang, and C. Zhu *et al*., "Static voltage stability margin prediction of island microgrid based on tri-training-LASSO-BP network," in *2020 IEEE Power & Energy Society General Meeting (PESGM)*, Montreal, QC, Canada, Aug. 2020, pp. 1-5.

[21] R. Tibshirani, "Regression shrinkage and selection via the LASSO," *Journal of the Royal Statistical Society: Series B (Methodological)*, vol. 58. no. 1, pp. 267-288, Jan. 1996.

[22] A. E. Hoerl and R. W. Kennard, "Ridge regression: applications to nonorthogonal problems," *Technometrics*, vol. 12, no. 1, pp. 69-82, Jan. 1970.

[23] J. Friedman, T. Hastie, and H. Hofling *et al*., "Pathwise coordinate optimization," *Annals of Applied Statistics*, vol. 1, no. 2, pp. 302-332, Jan. 2007.

[24] K. Tomsovic and M. Y. Chow," Tutorial on fuzzy logic applications in power systems," in *the IEEE-PES Winter Meeting in Singapore*, Singapore, Singapore, Jan. 2000.

[25] R. Babuska, "Fuzzy modeling and identification," Ph.D. Dissertation, Tech. Univ. Delft, Delft, The Netherlands, Jan. 1997.

[26] J.-S. R. Jang, "ANFIS: adaptive-network-based fuzzy inference system," *IEEE Transactions on Systems*, *Man*, *and Cybernetics*, vol. 23, no. 3, pp. 665-685, May 1993.

[27] A. Khusro, S. Husain and M. S. Hashmi, "Combining intelligence with rules for device modeling: approximating the behavior of AlGaN/GaN HEMTs using a hybrid neural network and fuzzy logic inference system," *IEEE Journal of the Electron Devices Society*, vol. 12, pp. 723-737, Sept. 2024.

[28] S. Jiriwibhakorn and K. Wongwut, "Evaluation of the power demand for economic load dispatch problem using adaptive neuro-fuzzy inference system and artificial neural network," *IEEE Access*, vol. 12, pp. 132352-132368, Sept. 2024.